JMEPEG (2012) 21:524–529
DOI: 10.1007/s11665-011-9931-2

1059-9495/$19.00

Corrosion Behavior of 35CrMn and Q235 Steel in Simulated Acid Rain Conditions

Xiu-li Zuo, Bin Xiang, Xing Li, and Zi-dong Wei

(Submitted June 9, 2010; in revised form March 14, 2011)

Effects of pH value, chloride ion concentration and alternation of wetting and drying time in acid rain on the corrosion of 35CrMn and Q235 steel were investigated through the measurement of polarization curves, electrochemical impedance spectroscopy, x-ray diffraction, and quantum mechanical calculations. The corrosion rate of 35CrMn and Q235 steel increased with decreasing pH values of the simulated acid rain, whereas the corrosion potential of 35CrMn and Q235 steel became more negative. The impedance became higher and the corrosion rate decreased with increasing test time. The dissolution rate of samples increased with chloride ion concentration. Results suggested that the corrosion rate of 35CrMn steel was obviously lower than that of Q235 steel for a more compact rust, α-FeOOH. Quantum chemical calculations further revealed that the increase in corrosion rate of the steel resulted from pitting corrosion caused by the corrosive chloride ion.

Keywords 35CrMn steel, electrochemical impedance spectroscopy, Q235, quantum chemical calculation, simulated acid rain

1. Introduction

Urban rapid rail transport, including railways and light rails, has become a convenient means of public transportation because it is fast, comfortable, safe, energy efficient, and environmentally friendly. However, most light rails are corroded when exposed to rain. In seriously polluted industrial cities, such as Chongqing, Guiyang, and other cities in China, rail corrosion has become an increasing concern because of acid rain (Ref 1-4). Light rails were not constructed using conventional steel railings, using instead reinforced concrete materials. Reinforced concrete rails are connected by pieces of 35CrMn metal plate, and Q235 steel nuts are used to fasten the metal plates. Our previous investigation showed that the 35CrMn steel connection metal plate and Q235 nut became corroded under atmospheric exposure for 1 year (Fig. 1). The corrosion behavior of 35CrMn and Q235 steel in simulated acid rain solution needs to be investigated for better selection criteria of materials suitable for urban construction, which can ensure safety and reduce maintenance costs.

2. Experimental

2.1 Composition of Simulated Acid Rain and Steels

Simulated acid rain was prepared according to the average composition of acid rain in the Chongqing area over the past 5 years (Ref 5) (Table 1). The pH value of the solution was adjusted by adding H_2SO_4 and HNO_3. The chemical composition of 35CrMn and Q235 steel (produced by Shougang group, China) is shown in Table 2.

2.2 Electrochemistry

A three-electrode system, consisting of a 35CrMn or Q235 steel as working electrode (WE), a saturated calomel electrode (SCE) as reference electrode, and a platinum plate as counter electrode (CE), was used for measurements. The WE was mounted by epoxy with an exposed area of 10×10 mm and then mechanically ground with a succession of emery papers ranging from grades 300 to 1000 before use. Finally, samples were washed with distilled water, degreased with alcohol and dried with cold air. Prior to polarization and impedance measurements, samples were immersed in a simulated acid rain solution for 1 h and dried in the air above the solution for about 11 h in a cycle. Electrochemical tests were conducted in simulated acid rain by an Auto-lab PGSTAT30 electrochemical analyzer system (Eco Chemie BV, Netherland). Anodic and cathodic polarization measurements were taken by potential dynamic methods at a potential range −0.8 to 0.3 V versus SCE with scan rate of 10 mV/min. Alternating current (AC) impedance measurements were performed at frequencies ranging from 3×10^{-3} to 10^5 Hz, with the magnitude of the applied AC signal at 10 mV. Impedance diagrams were obtained after about 30 min of immersion with a steady open circuit potential (OCP). The corrosion data of polarization curves and EIS were measured and analyzed by a general-purpose electrochemical system (GPES) and a frequency response analyzer (FRA) software. The rust layer on the samples was removed and analyzed by x-ray diffraction (XRD, D/max-3C, Japan).

3. Results and Discussion

3.1 Effect of pH of Simulated Acid Rain on Steel Corrosion

The polarization curves of 35CrMn and Q235 in simulated acid rain with different pH values (2.8, 3.8, 4.8, and 5.6) are shown in Fig. 2. The corresponding parameters are listed in

Xiu-li Zuo, Bin Xiang, Xing Li, and **Zi-dong Wei**, College of Chemistry and Chemical Engineering, Chongqing University, Chongqing 400044, China. Contact e-mail: xiangbin@cqu.edu.cn.

Table 3, where E_{corr} is the corrosion potential, i_{corr} is the corrosion current density, and R_p is the polarization resistance. The corrosion current densities of 35CrMn and Q235 steel increased with decreasing pH values, whereas the corrosion potentials of 35CrMn and Q235 steel gradually became negative; the polarization resistance correspondingly decreased. Results showed that the concentration of H^+ played a key role in the corrosion of steels in simulated acid rain because of the depolarization reaction of H^+ and O_2 under acidic conditions. The corrosion potential of metals in electrolytic solutions reflects the characteristics of the metal surface and the solution. Some anions adsorbed on the steel surface can increase its corrosion potential. Previous research has found that NO_3^- ions not only retard metal corrosion, but also increase the corrosion potential of metal (Ref 4). Some transient compounds on the metal surface or corrosion products can also raise the corrosion potential (Ref 6). As a result, the corrosion potentials of 35CrMn and Q235 steel shifted positively with an increase in pH values due to anion adsorption and surface corrosion product. The experiment showed that the corrosion resistance of 35CrMn was better than that of Q235, which was characterized by a more positive corrosion potential and a lower corrosion current.

3.2 Effect of Cl^- Concentration in Simulated Acid Rain on Steel Corrosion

According to literature (Ref 7), Cl^- can promote the anodic dissolution of steel. The effect of Cl^- concentration in simulated acid rain on 35CrMn steel corrosion was investigated, and the adsorption behavior of Cl^- on Fe surface was calculated by the Materials Studio software (MS). Based on Fig. 3, the anodic dissolution of steel was promoted by an increase in Cl^- concentration, and the corrosion potential of steel shifted negatively. At the same time, the corrosion current density increased. The Cl^- anion tended to adsorb on electrode surface defects and was so corrosive that pitting corrosion

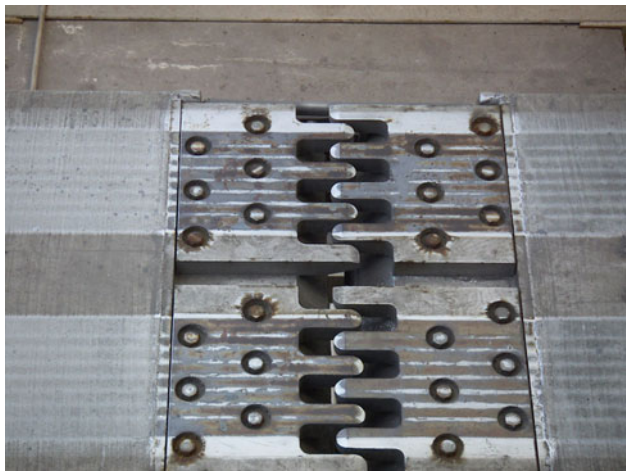

Fig. 1 Corrosion of light rail steels

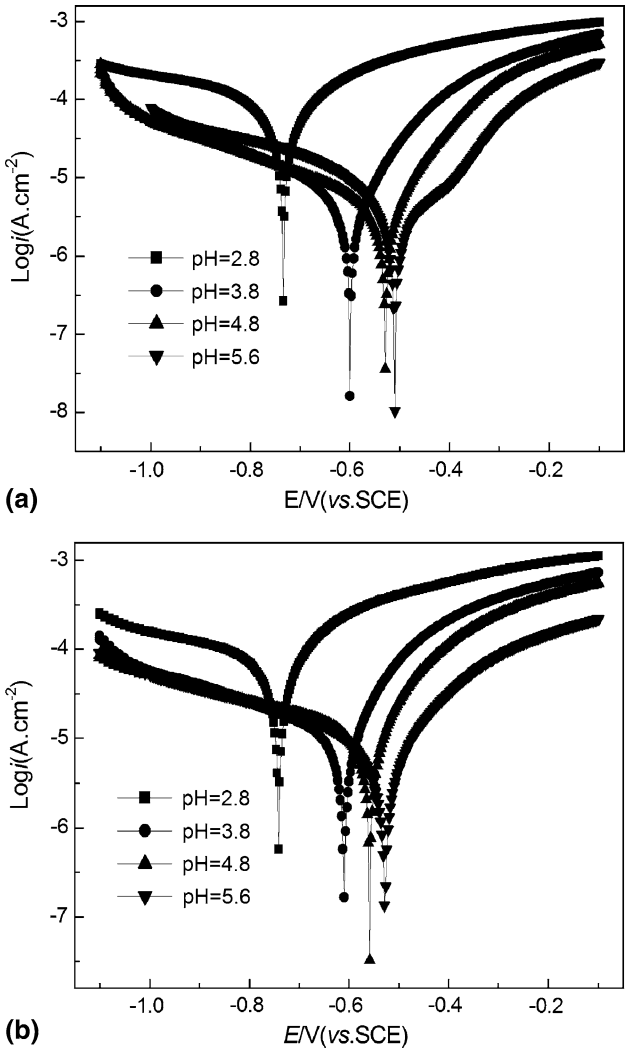

Fig. 2 Polarization curves of steel in simulated acid rain with different pH values (a) 35CrMn and (b) Q235

Table 1 Composition of simulated acid rain (mg/L)

SO_4^{2-}	NO_3^-	NH_4^+	Ca^{2+}	Mg^{2+}	Cl^-	K^+	Na^+	F^-
21.94	4.850	3.100	5.670	0.350	1.68	1.03	0.54	0.48

Table 2 Chemical composition of 35CrMn steel and Q235 (wt.%)

Element	C	Si	Mn	Cr	Ni	Cu	Mo	S	P	Fe
35CrMn	0.351	0.244	0.492	0.885	0.037	0.064	0.198	···	···	Bal.
Q235	0.17	0.26	0.46	···	···	···	···	0.017	0.0047	Bal.

Table 3 Corrosion parameters of steels in simulated acid rain with different pH values

pH	35CrMn			Q235		
	E_{corr}, V	i_{corr}, A/cm^2	R_p, Ω cm^2	E_{corr}, V	i_{corr}, A/cm^2	R_p, Ω cm^2
2.8	−0.734	1.481×10^{-5}	1.072×10^{3}	−0.741	2.086×10^{-5}	7.003×10^{2}
3.8	−0.600	1.970×10^{-6}	3.532×10^{3}	−0.610	4.310×10^{-6}	2.284×10^{3}
4.8	−0.529	1.451×10^{-6}	5.296×10^{3}	−0.558	4.050×10^{-6}	3.413×10^{3}
5.6	−0.509	1.029×10^{-6}	5.440×10^{3}	−0.528	2.208×10^{-6}	4.507×10^{3}

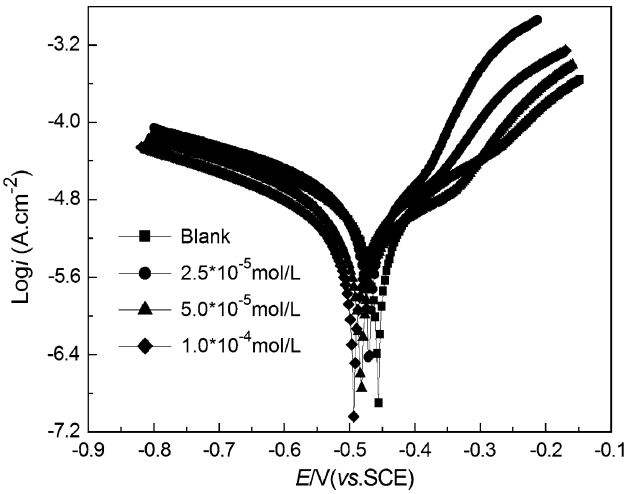

Fig. 3 Polarization curves of 35CrMn steel in simulated acid rain solution with different Cl^- concentrations. The blank is based on the composition of simulated acid rain

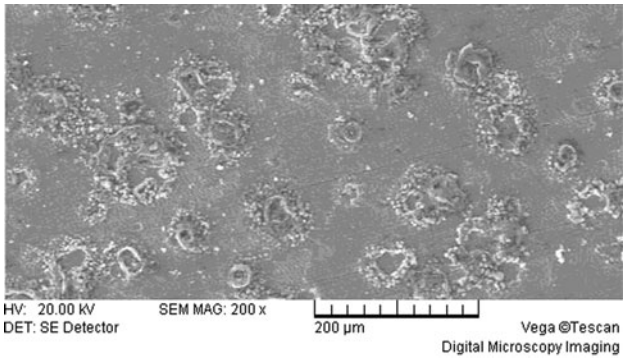

Fig. 4 SEM of 35CrMn steel after immersed in simulated acid solution for 18 h

occurred on the Fe surface (as shown in Fig. 4). Pitting corrosion was formed on the Fe surface with increasing Cl^- concentrations. Consequently, the corrosion rate of steel and the pitting corrosion increased with Cl^- concentration.

All quantum chemical calculations were performed using the Dmol3 module of the MS Software Package. Fully self-consistent density functional theory (DFT) calculations were employed in the present study. The generalized gradient spin approximation (GGA) and the function of Perdew and Wang (PW91) were used (Ref 8). A κ-point mesh of $6 \times 6 \times 1$ and $4 \times 4 \times 1$ was employed for a unit cell and Fe (111), respectively. The surface was cleaved by a bbc crystal structure of Fe, corresponding to Fe (111), and was composed of four Fe layers.

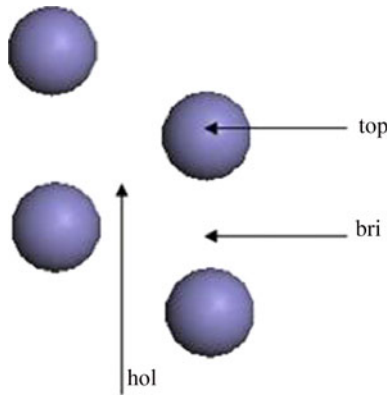

Fig. 5 Adsorption sites of Cl^- on Fe

To simulate ion adsorption, the two topmost layers of the slab were allowed to relax, while the two bottom layers were fixed. Chlorine ion adsorption was considered at a quarter monolayer coverage. Three-adsorption sites including the top, bridge and hollow sites were modeled as shown in Fig. 5.

The adsorption energies of Cl^- (E_{ads}) in the three-adsorption sites were calculated as follows:

$$E_{ads} = E_{ions/Fe\,(111)} - E_{ions} - E_{Fe\,(111)},$$

where E_{ions} and $E_{Fe\ (111)}$ represent the energy of Cl^- and Fe (111) substrate, respectively; and $E_{ions/Fe\ (111)}$ is the total energy of Cl^- adsorbed on the Fe surface. A positive E_{ads} indicates that adsorption was unfavorable, whereas a negative value indicates that adsorption is likely, with the lowest value being the most stable.

The adsorption energy values shown in Table 4 are all more negative than −40 kJ/mol, which indicates that Cl^- was chemically adsorbed in all three sites. The top site was the most favorable, which is in agreement with another report (Ref 7). Calculations showed that Cl^- could adsorb steadily on the metal surface and occupy the surface adsorption positions. Adsorption increased with an increase in Cl^- concentration, so anodic steel dissolution was also promoted. The optimized structure showed that the distance between the adsorbed Cl^- and the first layer of atoms ($\Delta Z_{Cl^-\cdot Fe}$ in Table 4) was different in the three-adsorption sites. The distances were determined to be 0.2368, 0.2060, and 0.2060 nm for the top, bridge, and hollow sites, respectively. However, the shortest bond distance between Cl^- and Fe ($d_{Cl^-\cdot Fe}$ in Table 4) was opposite to that of $\Delta Z_{Cl^-\cdot Fe}$. It showed that Cl^- ions could easily interact with the top site Fe atoms.

Yan et al. (Ref 7) indicated that the increasing adsorbed amounts of Cl^- tended to promote the loss of electrons of Fe atoms and its anodic dissolution due to the increased negative charges of $Fe(Cl^-)_{ads}$. A relaxation analysis of the Fe (111)

Table 4 Adsorption energies and structural optimization parameters of Cl^- on the Fe (111) surface at a quarter coverage

Parameter	E_{ads} (Cl^-), kJ/mol	$d_{Cl^-\cdot Fe}$, nm	$\Delta Z_{Cl^-\cdot Fe}$, nm	Δ, nm
Top site	−55.85	0.2368	0.2368	...
Bridge site	−42.83	0.2672	0.2060	0.0189
Hollow site	−42.82	0.2672	0.2060	0.0188

E_{ads} (Cl^-) is the adsorption energy, $\Delta Z_{Cl^-\cdot Fe}$ is the distance of Cl^- and the first layer atom, $d_{Cl^-\cdot Fe}$ is the distance of Cl^- and the closest Fe atom, Δ is the distance of movement of one Fe atom from the second layer of Fe atoms

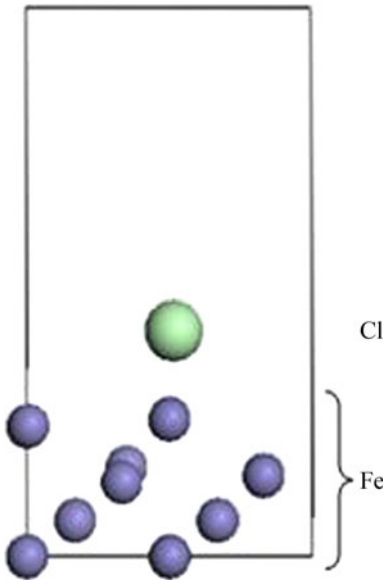

Fig. 6 Side view of the optimized adsorption model of Cl^- on Fe (111)

metal surface showed that the second atom layer moved as Cl^- was adsorbed on the Fe (111) surface at the bridge (Fig. 6) and hollow sites, but it did not move at the top site. The original crystal structure was destroyed when one of the second layer Fe atoms moved up on the surface at the bridge and hollow sites (Table 4). This could be the reason for the smaller adsorption energy observed at the bridge and hollow sites.

3.3 Effect of Exposed Time to Simulated Acid Rain on Steel

The electrochemical impedance spectroscopy results of 35CrMn and Q235 steel exposed in simulated acid rain at different time periods is quite different, which are shown in Fig. 7 as Nyquist plot and Fig. 8 as Bode plot. A single impedance semi-circle was found for 35CrMn steel at all sampling time from Fig. 7(a) and 8(a). The diameter of the impedance semi-circle decreased first and then increased with an increase in exposure time under the same pH value. The change of impedance might be due to the uneven corrosion of 35CrMn steel (shown in Fig. 4) at the beginning, and then more corrosion-resistant composition accumulated on the surface which led to impedance increase with immersion time increase. However, the impedance diagrams of Q235 were more complicated. It was presented a single deformed capacitive loop after one cycle in simulated acid solution that can be seen from Fig. 7(b) and 8(b). Maybe it was an anodic dissolution process of Q235 steel. A rusty layer which was fluffy, large porosity and incomplete on surface of Q235 steel was

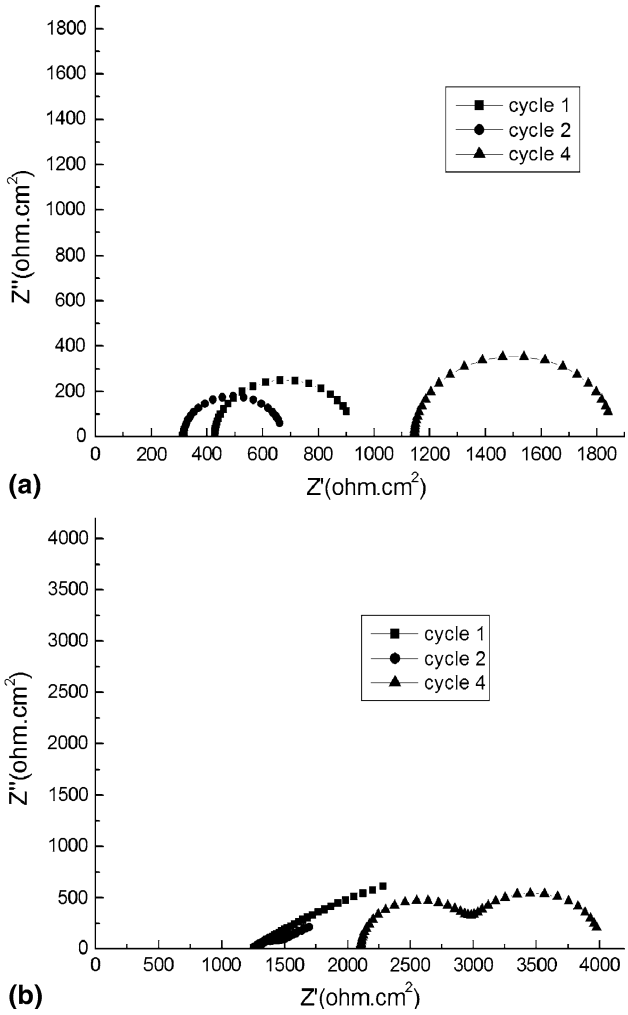

Fig. 7 Nyquist diagrams of steels with different exposure times in a simulated acid rain environment: (a) 35CrMn and (b) Q235

generated, and then much more corrosion product accumulated on the surface which had some protective effect on the steel matrix and leaded to impedance increase as immersion time increasing. It was improved such that rust inhibited the anodic dissolution of steel (Ref 9-11).

The difference of impedance performance as shown in above between Q235 and 35CrMn might be due to the different chemical composition of these two materials.

3.4 XRD Analysis of Rust

The microstructure of rust of 35CrMn and Q235 samples were studied by XRD. It showed that the phase components of

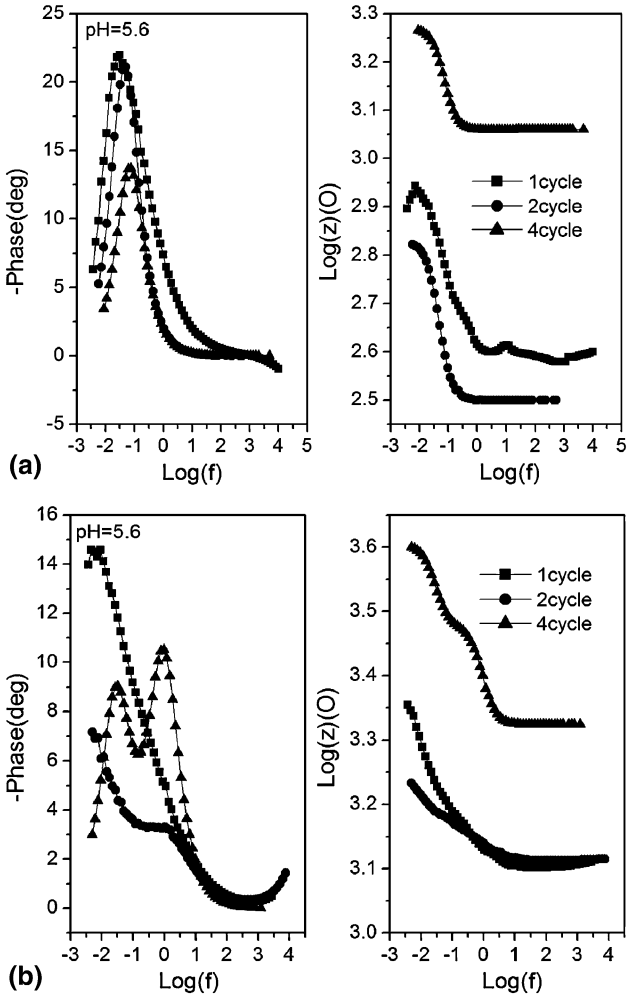

Fig. 8 Bode plots of steels with different exposure times in a simulated acid rain environment: (a) 35CrMn and (b) Q235

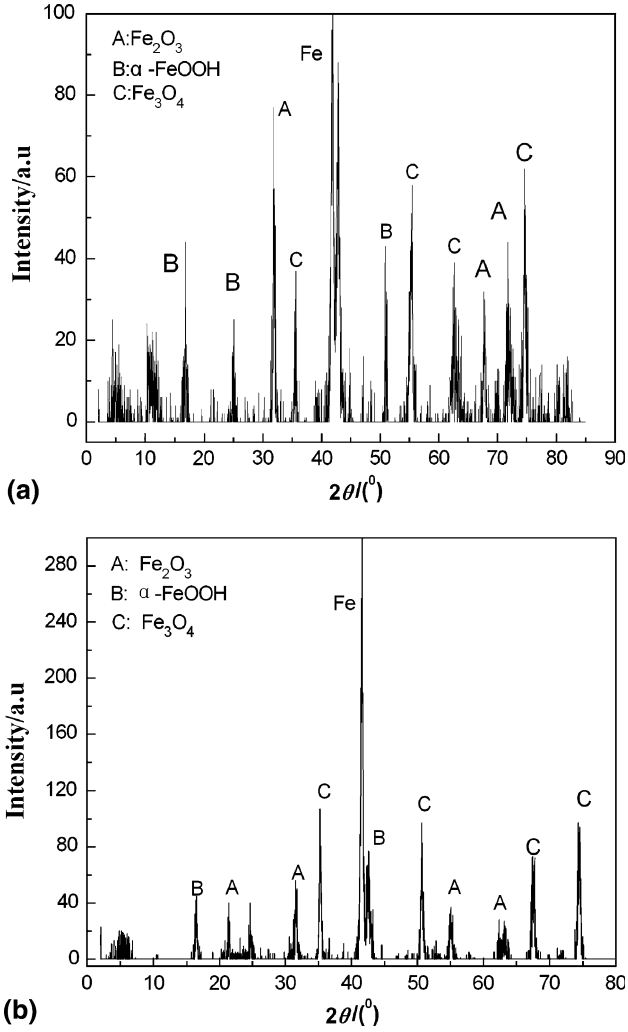

Fig. 9 XRD patterns of the rust layer of steel immersed in simulated acid rain for 72 h: (a) 35CrMn and (b) Q235

the rust layers on 35CrMn steel and Q235 steel were similar. They were composed primarily of α-FeOOH, Fe_2O_3, and Fe_3O_4 (Fig. 9).

A review of literature (Ref 12-14) confirmed that stable α-FeOOH rust can play a protective role to the steel matrix, but the Fe_2O_3 corrosion product, which was thick and porous, cannot protect the steel matrix. Zhang et al. (Ref 15) has proven that alloy elements lead to dense rusts. Results of the Raman spectra showed that the compact rust layer was composed of a Cr substituted-iron oxyhydroxide that could inhibit anion permeation into the metal matrix. Liu et al. (Ref 16) has employed electronic probe microscopy to confirm that the alloy element dissolved in rust could fill with corrosive holes and produce much stable corrosion products. Therefore, the corrosion resistance of 35CrMn was better than that of Q235 because of more alloy elements, such as Cr and Mn, which was in accordance with the above electrochemical behavior.

4. Conclusions

(1) The corrosion of 35CrMn in simulated acid rain was similar to that of Q235. With increasing pH, the corrosion current density gradually increased, and the E_{corr} shifted to a positive direction. The corrosion resistance of 35CrMn was better than that of Q235 steel, and the corrosion rate of 35CrMn decreased with corrosion time.

(2) The phase composition of the corrosion products of Q235 steel was similar to that of 35CrMn. The corrosion resistance of 35CrMn steel was better than that of Q235 because of the formation of the more stable α-FeOOH on the 35CrMn surface.

Acknowledgments

The authors are grateful for assistance of Project No. CDJRC 11220002 supported by the fundamental research funds for the central universities and the natural science for youth fund of Chongqing University.

References

1. B.G. An, X.Y. Zhang, H.E. Han et al., The Behavior of Corrosion and Runoff of A3 Steel in Artificial Rainwater, *Acta Metall. Sin.*, 2002, **38**(7), p 755–759 (in Chinese)

2. S. Magaion, M. Soga, K. Sobue et al., Zinc Corrosion in Simulated Acid Rain, *Electrochim. Acta*, 1999, **44**(24), p 4307–4312
3. Y.Y. Shi, Z. Zhang, J.X. Su et al., Electrochemical Noise Study on 2024-T3 Aluminum Alloy Corrosion in Simulated Acid Rain Under Cyclic Wet-Dry Condition, *Electrochim. Acta*, 2006, **51**(23), p 4977–4986
4. B.G. An, "Study on Corrosion Behavior of the Typical Metals in Rain/Acid Rain," Dissertation, Tianjin University, Tianjing, 2003, p 39 (in Chinese)
5. T.T. Hu, B. Xiang, X.L. Zuo et al., Corrosion Behavior of AZ91D Magnesium Alloy in Simulated Acid Rain, *Corros. Prot.*, 2009, **30**(7), p 477–479 (in Chinese)
6. Y.Q. Li, C. Sun, C.K. Yu et al., Influence of Simulated Sulfate Type Acid Rain on Corrosion Behavior of X70 Steel in Acidic Soil, *Corros. Sci. Prot. Technol.*, 2008, **20**(2), p 105–109 (in Chinese)
7. L.J. Yan, L. Niu, H.C. Lin et al., Quantum Chemistry Study on the Effect of Cl^- Ion on Anodic Dissolution of Iron in H_2S Containing Sulfuric Acid Solutions, *Corros. Sci.*, 1999, **41**(12), p 2303–2315
8. J.P. Perdew, K. Burke, and M. Ernzerhof, Generalized Gradient Approximation Made Simple, *Phys. Rev. Lett.*, 1996, **77**(18), p 3865–3868
9. B.S. Gu, X.C. Ji, M.S. Xia et al., Electrochemical Study on Rust of JT345 Economical Weathering Steel, *Corros. Prot.*, 2005, **26**(10), p 429–431 (in Chinese)
10. Q.C. Zhang, J.S. Wu, W.L. Zheng et al., Stabilization Process of Rust Layer on Surface of Weathering Steel, *Shanghai Met.*, 2004, **26**(3), p 10–12 (in Chinese)
11. Q.C. Zhang, J.S. Wu, W.L. Zheng et al., Effect of Ion Selective Property on Protective Ability of Rust Layer Formed on Weathering Steel Exposed in the Marine Atmosphere, *Acta Metall. Sin.*, 2001, **37**(2), p 193–196 (in Chinese)
12. J.T. Keiser, C.W. Brown, and R.H. Heidersbach, The Oxidation of Fe_3O_4 on Iron and Steel Surfaces, *Corrosion*, 1982, **38**(7), p 357–360
13. M. Stratmann and K. Hoffmann, In situ Mossbauer Spectroscopic Study of Reactions Within Rust Layers, *Corros. Sci.*, 1989, **29**(11–12), p 1329–1352
14. T. Kamimura, S. Nasu, T. Tazaki et al., Mossbauer Spectroscopic Study of Rust Formed on a Weathering Steel and a Mild Steel Exposed for a Long Term in an Industrial Environment, *Mater. Trans.*, 2002, **43**(4), p 694–703
15. Q.C. Zhang, J.S. Wu, J.J. Wang et al., Corrosion Behavior of Weathering Steel in Marine Atmosphere, *Mater. Chem. Phys.*, 2003, **77**(2), p 603–608
16. G.C. Liu, J.H. Dong, H.E. Han et al., Influence of Cu and Mn on Corrosion Behavior of Low Alloy Steel in a Simulated Coastal Environment, *Corros. Sci. Protect. Technol.*, 2008, **20**(4), p 235–238 (in Chinese)